All-Optical Nonlinearities in Organics

B. I. GREENE, J. ORENSTEIN, S. SCHMITT-RINK

Recognition that organic solids possess some of the largest all-optical nonlinearities of all known materials has resulted in an interdisciplinary effort directed at both the basic understanding and exploitation of these effects. Parallel efforts on inorganic semiconductors have already reached a mature stage whereby the origin of the effects, together with the prospects for device applications, are well known and appreciated. In this article, a unified picture of nonlinear optical phenomena in both classes of materials is presented. The specific implications for organic-based optical devices are discussed.

WITH THE ADVENT OF LASERS AND THE CONSEQUENT availability of high-intensity monochromatic light, the new field of "nonlinear optics" was born (*1*). A wealth of phenomena pertaining to the interaction of light with matter quickly emerged (*2, 3*). From the point of view of the general scientific community, however, the distinction between the fields of "optics" and "nonlinear optics" has been an unfortunate one. Where optics is a subject well appreciated and easily imagined, nonlinear optics carries an aura of conceptual obtuseness and mathematical intricacy. The wealth of phenomena has created this aura, and it is the purpose of this paper to, in a limited and somewhat pragmatic fashion, point out the forest for the trees.

The age of optical telecommunications has begun, and we ask which, if any, nonlinear optical effects are likely to play a role. At present, the well-established technology is one in which digital electrical signals are converted into pulses of light by rapidly turning semiconductor lasers on and off. The resultant optical data stream is launched down optical fibers and received by a solid-state detector at the other end, at which point the optical bit stream is reconverted to digital electrical impulses. Subsequent switching and signal processing is, by and large, performed by conventional electronic means. Optical telecommunications today therefore really refers to optical data transmission, with the realization that transmission is only one part of an overall telecommunication system.

A logical next step in the development of an optical telecommunication system would be to provide a direct means of switching optical data lines without conversion back to electronic pulses. The control signals for such a switch could initially be electrical, and ultimately optical. It is these "all-optical" devices, and the phenomena on which they are based, that many consider to be both the most experimentally challenging and potentially the most technologically revolutionary.

All-optical devices rely on nonlinear optical materials. For the purposes of the present discussion we define a nonlinear optical material as any material that changes any of its optical properties when light is shined upon it. We quantify these changes by examining the behavior of the optical constants upon photoexcitation. These constants describe the optical response of a material and are most familiar as the frequency-dependent absorption coefficient α and refractive index n. Usually such devices are interferometric in design, a configuration in which small changes Δn in refractive index can lead to large changes at the output of the device.

It is important to make the distinction between "resonant" and "nonresonant" nonlinear optical effects (*4*). Resonant effects are large and are the direct result of elementary excitations created in a material by the absorption of incident light. Excitations so created are considered "real" in the sense that they have a lifetime and result in the permanent scattering of energy out of the light field and into the material. Nonresonant nonlinear optical effects are small and differ in that elementary excitations are created only "virtually" and hence no light is absorbed. They result from the spontaneous distortion of the electronic wavefunctions in the presence of the laser field. Once the field is turned off, the electrons revert to their unperturbed configuration. Nonresonant response times are necessarily short.

By the mid-1970s, it was recognized that solids composed of certain types of organic molecules exhibit anomalously large nonresonant nonlinear optical properties (*5*). The prospect of incorporation of these materials in a new class of all-optical devices was an exciting one that attracted many researchers. Almost 20 years later, very little tangible progress toward this goal has been realized. In what follows, we discuss the basic physical principles governing the all-optical nonlinear effects in the organics and draw conclusions pertaining to the ultimate use of such effects and materials.

The Approach

Recent progress in nonlinear optical phenomenology applied to inorganic semiconductors has prompted us to adopt a similar formalism for optical nonlinearity in the organics. Over the years, great effort has been directed toward the development and understanding of nonlinear optical materials. Two parallel yet largely noninteracting communities have individually concentrated on organic and inorganic materials. A major goal of our work has been to unify these two fields with one simple theoretical model, discuss how the materials differ or are alike in their nonlinear optical properties, and appraise their device potential in the context of this unified picture. We are confident that this approach will be successful, because we believe that the same basic quantum mechanical picture should be able to describe all solids, whether the solid be comprised of gallium and arsenic, or carbon, nitrogen, and hydrogen.

The authors are at AT&T Bell Laboratories, Murray Hill, NJ 07974.

In what are now classic investigations, accurate quantitative measurements performed on high-quality GaAs samples recorded the change in optical constants in response to an incident light field (*6*). This work explored both the response of bulk samples and, more recently, the response of reduced dimensional or quantum confined structures. A simple theory, based on an "exclusion principle," capable of quantitatively predicting saturation of optical transitions in response to either resonant or nonresonant incident radiation, has been successful in explaining numerous experimental observations in systems fabricated with GaAs. In terms of bulk GaAs and two-dimensional (2-D) quantum-confined structures, there remains today little uncertainty as to what and how large the optical nonlinearities are (*6*). We wish to be able to say the same for the organics and, with this goal in mind, set out to quantify the nonlinear optical response of a model organic system.

Large all-optical nonlinear effects have often been associated with π-bonded, electron-delocalized organic molecules. Numerous qualitative and quantitative theoretical discussions have been presented rationalizing this observation (*3*). From our point of view, the major relevant fact is that oscillator strength is concentrated into low-lying electronic transitions as a consequence of a reduced dimensional (in this case quasi–1-D) electronic structure. However, the amount of oscillator strength in a particular optical transition cannot exceed the sum of the oscillator strengths of the constituent atoms. As will be discussed in detail below, this effectively puts limits on the ultimate magnitude of the nonlinear optical response. We believe the molecule polydiacetylene (PDA) to be close to this limit.

Polydiacetylene is a polymer, can be prepared in single crystalline form, and should not be confused with polyacetylene. The structures of the two polymer backbones are shown in Fig. 1. The realization that polyacetylene has a degenerate ground state giving rise to a unique class of fundamental excitations called solitons generated a tremendous amount of excitement about this latter material (*7*). Polyacetylene has yet to be prepared as a single crystal though, making it considerably less useful than PDA as a model system for nonlinear optical studies. Although PDA is a polymer, for reasons that will become clear, we wish to de-emphasize this aspect with regard to the "ultimate" nonlinear optical response. Our results should prove general to all molecular crystals, be they polymeric or comprised of discrete molecules.

Several different PDA molecules have been crystallized. By far the most extensively characterized is designated PDA-pTS, where "pTS" abbreviates a "para-toluene-sulfonate" side group designated "R" in Fig. 1 (*8*).

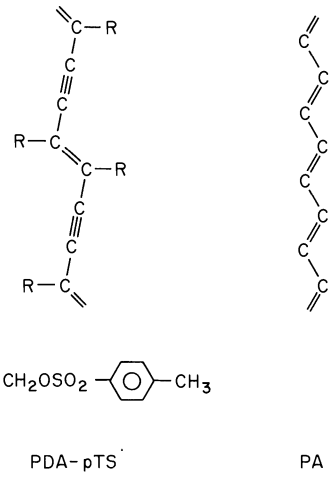

Fig. 1. Molecular structure of polydiacetylene-paratoluene-sulfonate (PDA-pTS) and polyacetylene (PA).

Preliminary Considerations: Two-Level Systems

The susceptibility tensors $\chi^{(n)}$ are the formal embodiment of a materials nonlinear optical response. The electric field associated with incident light induces a polarization P which is, in the simplest case, linearly related by way of the proportionality constant χ. For sufficiently large electric fields, however (such as those associated with intense laser light pulses), the general observation has been that the microscopic charges comprising matter fail to respond to the applied field in a strictly linear way. The polarization can more generally be expressed in expanded powers of E,

$$P = \chi^{(1)}E + \chi^{(2)}E^2 + \chi^{(3)}E^3 + \cdots + \chi^{(n)}E^n \qquad (1)$$

All-optical nonlinear optical phenomena are described by the fourth-rank tensor $\chi^{(3)}$ (*9*). This tensor has $3^4 = 81$ elements in cartesian coordinates that describe the interaction of light with all one and two electron-hole pair states in the material. For any particular incident light wavelength, the various elements will vary in absolute magnitude. The task of evaluating the overall cubic nonlinear optical response could be vastly simplified if one could separate the 81 individual contributions into two groups: those relatively large, and those relatively small. One would then ignore all the small contributions and approximate $\chi^{(3)}$ by calculating the less numerous but more significant terms.

Polydiacetylene-pTS has the largest measured value of the nonresonant nonlinear refractive index n_2 of any solid (n_2 is defined through $\Delta n = n_2 I$, where I is the light intensity) (*5, 10*). The linear optical properties of PDA-pTS are striking because of the existence of a spectrally narrow and intense lowest lying electronic absorption (see below and Fig. 4) (*11*). Other materials, both organic and inorganic, that have been observed to have significant nonresonant values of n_2 can also be described qualitatively as having strong low-lying electronic transitions (*12*). We suggest that the large optical nonlinearities of these materials are a primary consequence of these optical transitions and attempt first to understand and model the nonlinear optical response in the context of a simple two-level system (*13*). The two-level system model is the simplest theoretical approach to nonlinear optics and one that we will demonstrate is basically sufficient to explain the most important practical aspects of the observed nonlinear effects in many organic and inorganic materials.

More specifically, the two levels in this model might correspond to the bonding and anti-bonding orbitals that form the highest valence (v) and lowest conduction (c) bands (or, in the case of a

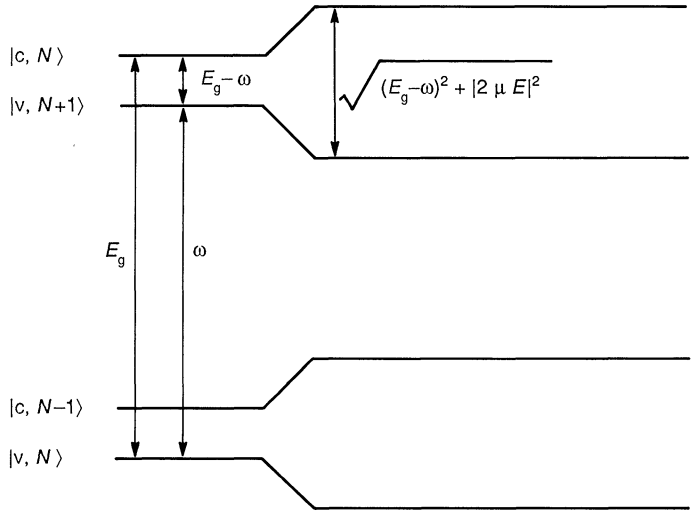

Fig. 2. Dressed two-level atom states.

molecular crystal, to the ground and first excited electronic state). We denote the lower level by |v>, the upper one by |c>, and the energy gap $\epsilon_c - \epsilon_v$ by E_g (see Fig. 2). The Hamiltonian describing the interaction with the light field is given by

$$H_{\text{dipole}} = -\mu E(t)|c><v| - \text{h.c.} \quad (2)$$

where μ is the dipole matrix element and "h.c." stands for the Hermitian conjugate. (Here and in the following, we omit the spatial indices.)

For monochromatic laser fields $E(t) = E\exp(-i\omega t)$, there are two completely equivalent approaches to the nonlinear optical response of such a system: (i) the bare states approach and (ii) the dressed states one (*13*). The latter often provides simple physical explanations of nonlinear optical phenomena more easily. Eliminating the time dependence of the Hamiltonian by a unitary transformation, one finds, after diagonalization, the dressed levels shown in Fig. 2 ($\hbar = 1$). The physics underlying this spectrum is straightforward: the state with the electron in |v> and, say, $N + 1$ photons is (almost) degenerate with the state with N photons and the electron in |c>. The dipole interaction couples the two states and leads to the usual level repulsion and splitting. Similar arguments explain the lower doublet in Fig. 2. In analogy to the shift or splitting of energy levels in a static (dc) electric field, this all-optical effect is often referred to as the dynamical (ac) Stark effect.

The most general experimental measurement of an all-optical (third-order) nonlinearity requires two incident light beams and a sample. The first beam is relatively strong; that is, strong enough to induce an appreciable nonlinear optical response. This beam is often referred to as the "pump beam." A second "probe beam," of considerably lower intensity, measures the change in optical properties of the sample.

According to Fig. 2, the absorption of a weak probe beam should be considerably modified in the presence of a strong pump beam, showing, for instance, a blue-shifted transition under nonresonant excitation ($\omega < E_g$). This ac Stark shift, as well as many other interesting phenomena, have been extensively studied over the last two decades in atomic vapors. More recently, some of these effects have also been observed in inorganic semiconductors and PDA-pTS (see below).

The explicit calculation of the nonlinear optical response is conveniently performed with the bare states approach, which leads to Bloch equations, initially developed in the theory of magnetic resonance (*13*). Introducing the density matrix ρ_{ab}, where {a,b} = {c,v}, of the two-level system, one can easily derive the coupled equations for the induced polarization $P = \mu^*\rho_{vc}$ and excited state population $f = \rho_{cc} = 1 - \rho_{vv}$. Including phenomenological transverse and longitudinal relaxation rates γ_2 and γ_1, respectively, one finds

$$\frac{\partial}{\partial t}P(t) = -iE_gP(t) + i|\mu|^2[1 - 2f(t)]E(t) - \gamma_2P(t) \quad (3)$$

and

$$\frac{\partial}{\partial t}f(t) = i[P^*(t)E(t) - P(t)E^*(t)] - \gamma_1 f(t) \quad (4)$$

These equations may now be solved in arbitrary order in the electric field $E(t)$ to give the nonlinear susceptibilities $\chi^{(n)}$.

In order to describe pump and probe experiments, we split the laser field into a strong pump (p) and a weak test (t) field, $E(t) = E_p(t) + E_t(t)$, and linearize Eqs. 3 and 4 with respect to $E_t(t)$ (*14*). The resulting induced polarization has components oscillating at the three frequencies ω_p, ω_t, and $2\omega_p - \omega_t$. We denote them by $P_p(t)$, $P_t(t)$, and $P_s(t)$, respectively. $P_p(t)$ and $P_t(t)$ are the polarizations induced by the pump and probe beams, while $|P_s(t)|^2$ describes the (four-wave mixing) signal generated parametrically. The latter shall not concern us here. The linear and third-order polarizations $P^{(1)}_{p,t}(t)$ and $P^{(3)}_{p,t}$ satisfy the equations

$$\frac{\partial}{\partial t}P^{(1)}_{p,t}(t) = -iE_gP^{(1)}_{p,t}(t) + i|\mu|^2E_{p,t}(t) - \gamma_2P^{(1)}_{p,t}(t) \quad (5)$$

$$\frac{\partial}{\partial t}P^{(3)}_{p}(t) = -iE_gP^{(3)}_{p}(t) - 2i|\mu|^2f^{(2)}(t)E_p(t) - \gamma_2P^{(3)}_{p}(t) \quad (6)$$

and

$$\frac{\partial}{\partial t}P^{(3)}_{t}(t) = -iE_gP^{(3)}_{t}(t) - 2i|\mu|^2f^{(2)}(t)E_t(t) - 2i|\mu|^2\Delta f^{(2)}(t)E_p(t) - \gamma_2P^{(3)}_{t}(t) \quad (7)$$

where

$$\frac{\partial}{\partial t}f^{(2)}(t) = i[P_p{}^{(1)*}(t)E_p(t) - P^{(1)}_p(t)E^*_p(t)] - \gamma_1 f^{(2)}(t) \quad (8)$$

and

$$\frac{\partial}{\partial t}\Delta f^{(2)}(t) = i[P^{(1)*}_p(t)E_t(t) - P^{(1)}_t(t)E^*_p(t)] - \gamma_1\Delta f^{(2)}(t) \quad (9)$$

For monochromatic laser beams, Eqs. 5 to 9 may be readily solved to give the susceptibilities (per two-level system) experienced by the pump and probe beams [$\chi^{(n)}_{p,t} = P^{(n)}_{p,t}(t)/E_{p,t}(t)$] (*15*)

$$\chi^{(1)}_{p,t} = \frac{|\mu|^2}{E_g - \omega_{p,t} - i\gamma_2} \quad (10)$$

$$\chi^{(3)}_p = -\chi^{(1)}_p\frac{2|\mu|^2}{(E_g - \omega_p)^2 + \gamma_2{}^2}\frac{2\gamma_2}{\gamma_1} \quad (11)$$

and

$$\chi^{(3)}_t = -\chi^{(1)}_t\left[\frac{2|\mu|^2}{(E_g - \omega_p)^2 + \gamma_2{}^2}\frac{2\gamma_2}{\gamma_1} - \frac{2|\mu|^2}{\omega_t - \omega_p + i\gamma_1} \times \left(\frac{1}{\omega_t - E_g + i\gamma_2} - \frac{1}{\omega_p - E_g - i\gamma_2}\right)\right] \quad (12)$$

Equations 10 and 11 show that for any given pump frequency the absorption of the pump beam $\alpha_p \sim \text{Im}\chi^{(1)}_p + \text{Im}\chi^{(3)}_p|E_p|^2$ decreases with pump intensity. This decrease is due to the (incoherent) population induced by the pump [$f^{(2)}$] and is a consequence of the Pauli exclusion principle: states that are already occupied are no longer accessible in optical transitions. The absorption of the probe beam $\alpha_t \sim \text{Im}\chi^{(1)}_t + \text{Im}\chi^{(3)}_t|E_p|^2$ contains an additional term (second term on the right-hand side of Eq. 12) due to the (coherent) population modulation induced by both the pump and the probe [$\Delta f^{(2)}$]. This term describes the scattering of the pump beam (i) off the grating created by interference with the probe and (ii) into the direction of the probe. It redistributes the probe absorption, but does not reduce its integrated value.

In Figs. 3, a and b, we have plotted α_t in the absence (dashed lines) and presence (full lines) of the pump for resonant (Fig. 3a) and nonresonant (Fig. 3b) excitation. The excited state population was kept constant at a value of 0.0625 (*15*). For resonant excitation (Fig. 3a) and in the absence of proper dephasing ($\gamma_1 = 2\gamma_2$), the profile of α_t is similar to that of the linear absorption, with both population and population modulation terms giving rise to saturation near the line center. In fact, for $\omega_t = \omega_p$, the absorption saturation of the probe beam is twice as large as that of the pump. In contrast, in the presence of proper dephasing ($\gamma_1 = 0.1\gamma_2$), a narrow hole of half width at half maximum (HWHM) $\sim \gamma_1$ centered at the pump frequency is "burned" into the (homogeneous!) absorption

line. For $\omega_t = \omega_p$, the saturation of the test beam absorption is the same as previously, while for $|\omega_t - \omega_p| > \gamma_1$ the population can no longer follow the beat between pump and probe, so that the contribution of the population modulation term diminishes. For nonresonant excitation (Fig. 3b), α_t exhibits again saturation due to the pump-induced population and, depending on the value of γ_1, a more or less pronounced ac Stark shift, as expected on the basis of Fig. 2. For $\gamma_1 = 0.1\gamma_2$, the population modulation-induced feature at the pump frequency now has a dispersive shape. Below, we shall encounter a similar behavior in PDA-pTS.

The Model Organic Response

Accurate determination of a materials response to optical stimulus ideally requires an ability to create and measure a change in optical properties in a period comparable to or shorter than the characteristic relaxation time of that change. Previous time-resolved kinetic studies performed in PDA-pTS have measured the resonant longitudinal relaxation time γ_1 to be on the order of ~2 ps, making necessary the use of ultrashort pulsed lasers to obtain the desired data (*16, 17*). We have performed our spectroscopic measurements with a laser system that produced ~100-fs temporal duration optical pulses tunable in wavelength between 550 and 780 nm (*18*). These pulses are of sufficient energy that when focused into a continuous medium, they are capable of producing a broad-band white light "continuum" pulse of equally short temporal duration. The continuum pulses are used as a probe that enables ~100-fs spectroscopic "snapshots" to be taken of the sample. The subpicosecond time resolution of this technique is purely a consequence of the ultrashort laser pulses and relies in no way on fast optical detectors or electronics. By starting with one laser pulse, dividing it into two (pump and probe) and changing the pathlength by ~1 mm that the pump pulse has to travel before reaching the sample relative to that of the probe pulse, one has changed the relative time delay between excitation and probing by ~3 ps. The instrumental time response of such a technique is on the order of the laser pulsewidth, in our case roughly ~100 fs.

We set out to explore the resonant response of our archtypical organic crystal, PDA-pTS. The bottom of Fig. 4 displays a differential absorption spectrum of PDA-pTS taken slightly after (~0.2 ps) resonant pulsed excitation (*18*). The resonant excitation ($\omega_p \sim 2$ eV) differential signal was observed to decay with roughly a ~2 ps time constant. The top of the figure displays the linear absorption spectrum (optical density OD = $\alpha_t L$, where L is the sample thickness) of the ~200 Å thick sample, and was taken with a low-intensity cw white light source. The linear optical absorption is dominated by an exciton (x) peak at $E_x \sim 2$ eV of HWHM $\gamma_2 \sim 50$ meV, consistent with results obtained previously by Kramers-Kronig analysis of bulk crystal reflectivity (*11*). We note that the exciton oscillator strength is so large that the linear absorption lineshape is considerably distorted from $\mathrm{Im}\chi^{(1)}$ (*19*). The peak absorption ($\sim 10^6$ cm^{-1}) is about two orders of magnitude higher than in GaAs, as is the exciton binding energy (~0.4 to 0.5 eV).

In separate sets of measurements, we have explored the nonlinear optical response of PDA-pTS as a function of pump detuning in between the regions of resonance and off-resonance (2.0 to 1.6 eV) (*18*). The right-hand side of Fig. 5 displays several temporal traces monitoring the change in optical density at ~620 nm (the peak of the excitonic absorption) as a function of delay time between pump and probe. The traces have been offset and positioned so that the temporal peak of the response occurs at the wavelength of excitation. The excitation intensity was held constant for all excitation wavelengths at $I_p \sim 3$ GW cm^{-2}. On the left of Fig. 5 is the sample linear absorption spectrum. As the excitation wavelength is tuned off and away from the linear absorption tail, several notable observations are made. Excitation on the absorption edge (at 640 nm, for example) results in a reduction of absorption (at 620 nm) that manifests a finite relaxation time of ~2 ps. As one tunes below the peak of excitonic absorption, the spectroscopic response becomes smaller in magnitude and shorter in lifetime. By 680 nm excitation, the response has become instantaneous, that is, resolution limited. The magnitude of the response at this point however begins to increase and in fact shows maxima at the excitation wavelengths of 690 and 720 nm. The full differential spectrum taken simultaneous with 690 nm excitation ($\omega_p \sim 1.8$ eV) is shown in the center of Fig. 4. We note the difference between it and the differential spectrum taken with resonant excitation (bottom). The magnitude of the

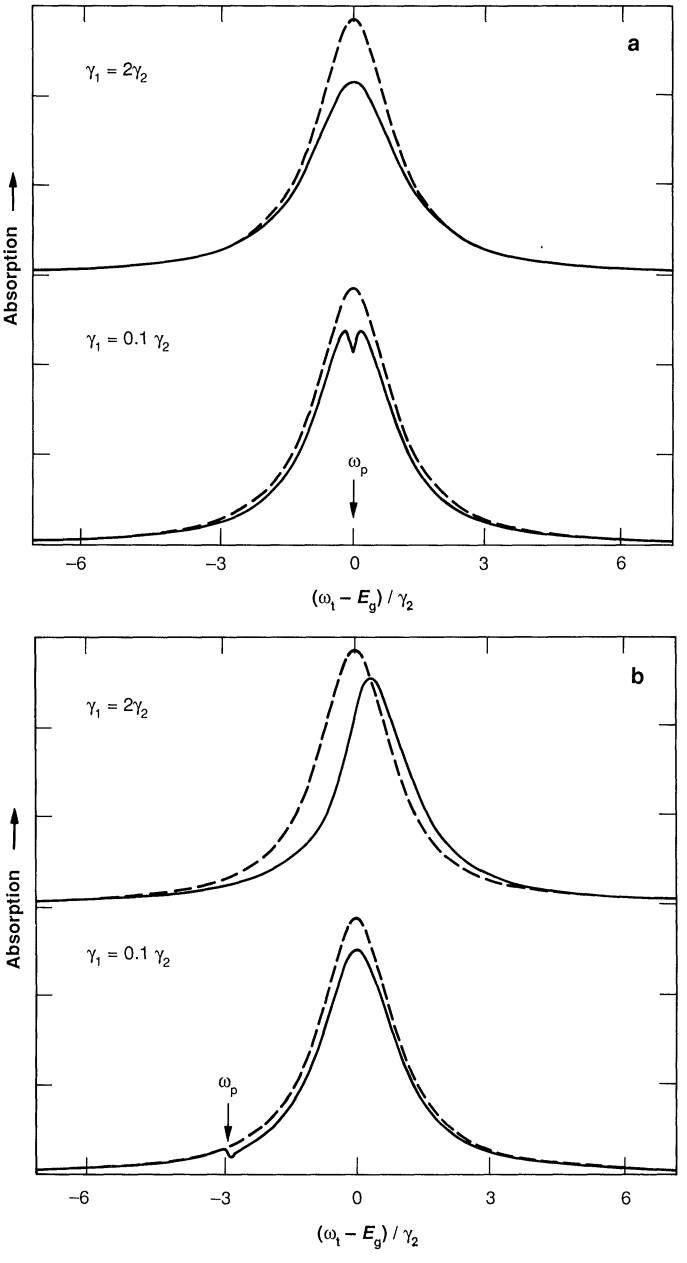

Fig. 3. Linear (dashed lines) and nonlinear (full lines) absorption spectra of two-level atoms excited (**a**) on resonance and (**b**) ~$3\gamma_2$ below resonance, in the absence ($\gamma_1 = 2\gamma_2$) and presence ($\gamma_1 = 0.1\gamma_2$) of proper dephasing. Pump and probe beams were assumed to be monochromatic, and the excited-state population was kept constant at a value of 0.0625.

instantaneous response shown as a function of pump detuning from the exciton resonance in Fig. 6 reveals two maxima occurring at energies close to that of optic phonons (indicated by arrows). These two phonons are known from resonance Raman spectroscopy to be the two which couple most strongly to the exciton (*11*). They are also apparent in the linear absorption, where they give rise to phonon satellites on the high-energy side of the exciton resonance.

Extension of the Two-Level Model

The observed exciton absorption saturation under resonant excitation resembles that of two-level systems (Fig. 3a). In order to describe it, we make use of the phase-space filling (PSF) model employed previously to explain similar effects in bulk and quantum confined GaAs at low temperatures (*6*). This model is a straightforward extension of our previous discussion to the case of N hybridized and interacting two-level atoms. It ignores certain phenomena (to be discussed below), but demonstrates very clearly some of the fundamental limits on nonlinear optical susceptibilities.

In a one-dimensional (1-D) crystal with N atoms, we have to replace Eq. 2 by

$$H_{\text{dipole}} = -\mu E(t)\sum_i |ci><iv| - \text{h.c.} \tag{13}$$

where $|ci>$ and $|vi>$ are Wannier orbitals localized at the atomic sites z_i. Using

$$|\alpha i> = \frac{1}{N^{1/2}}\sum_k \exp(-ikz_i)|\alpha k> \; ; \; \alpha = \text{c, v} \tag{14}$$

we transform Eq. 13 into the Bloch representation

$$H_{\text{dipole}} = -\mu E(t)\sum_k |ck><kv| - \text{h.c.} \tag{15}$$

In the absence of Coulomb interaction, it is now easy to generalize our previous results, because each individual valence to conduction band transition with given k behaves in much the same way as a two-level system. The crystal as a whole behaves like an inhomogeneously broadened one, with the inhomogeneous broadening given by the joint density of states.

The Coulomb interaction modifies this picture in several ways. As for the linear optical absorption, it couples the electron (e) promoted into the conduction band with the hole (h) left behind in the valence band, to give bound and scattering exciton states. In the Bloch representation, the generalization of Eq. 5 for the linear polarization $[P(t) = \sum_k P_k(t)]$ reads

$$\frac{\partial}{\partial t} P_k^{(1)}(t) = -i(\epsilon_{ck} - \epsilon_{vk})P_k^{(1)}(t) + i$$
$$\left[|\mu|^2 E(t) + \sum_{k'} V_{k,k'} P_{k'}^{(1)}(t)\right] - \gamma_2 P_k^{(1)}(t) \tag{16}$$

where $V_{k,k'}$ is the Coulomb matrix element. Thus, an e-h pair with a given k does not only experience the external field $E(t)$, but also a significant internal one, the "molecular" field associated with e-h pairs created at k'. At each k, external and Coulomb field combine to give an effective self-consistent "local" field to which the system responds.

Equation 16 is an inhomogeneous Wannier-Schroedinger equation, driven by the laser field $E(t)$ and including a phenomenological transverse relaxation rate γ_2. It can be solved by expanding $P_k(t)$ in terms of the stationary solutions of the corresponding homogeneous equation

$$\sum_{k'}\left[(\epsilon_{ck} - \epsilon_{vk})\delta_{k,k'} - V_{k,k'}\right]\phi_n(k') = E_n\phi_n(k) \tag{17}$$

This yields Elliott's formula for the linear optical susceptibility (*20*)

$$\chi^{(1)} = \frac{N}{V}\sum_n \frac{|\mu\phi_n(z_j = 0)|^2}{E_n - \omega - i\gamma_2} \tag{18}$$

where V is the total active volume ($V/N \sim 500$ Å^3 in PDA-pTS). For a short-range interaction, one finds for the lowest exciton state (n = x)

$$\phi_x(z) \sim \left(\frac{a}{a_x}\right)^{1/2} \exp\left(-\frac{|z|}{a_x}\right) \tag{19}$$

where we have assumed an exciton Bohr radius a_x larger than the lattice constant a ($a \sim 5$ Å in PDA-pTS) and taken the continuum limit. Substituting this result into Eq. 18, we see that the total oscillator strength in the lowest exciton resonance is given by

$$|\mu_x|^2 = \frac{a}{a_x} N|\mu|^2 \tag{20}$$

which is bounded by the 1 and N atom values. Frenkel excitons ($a_x \sim a$) have a very large dipole moment ($\sim N^{1/2}$), while the dipole moment of Wannier excitons ($a_x >> a$) is reduced beyond this value by the fraction of the Brillouin zone that participates in the exciton orbital wave function.

The $\sim N^{1/2}$ scaling of the exciton dipole moment has led to the suggestion that $\chi^{(3)}$ should scale like $\sim N^2$, as long as phase

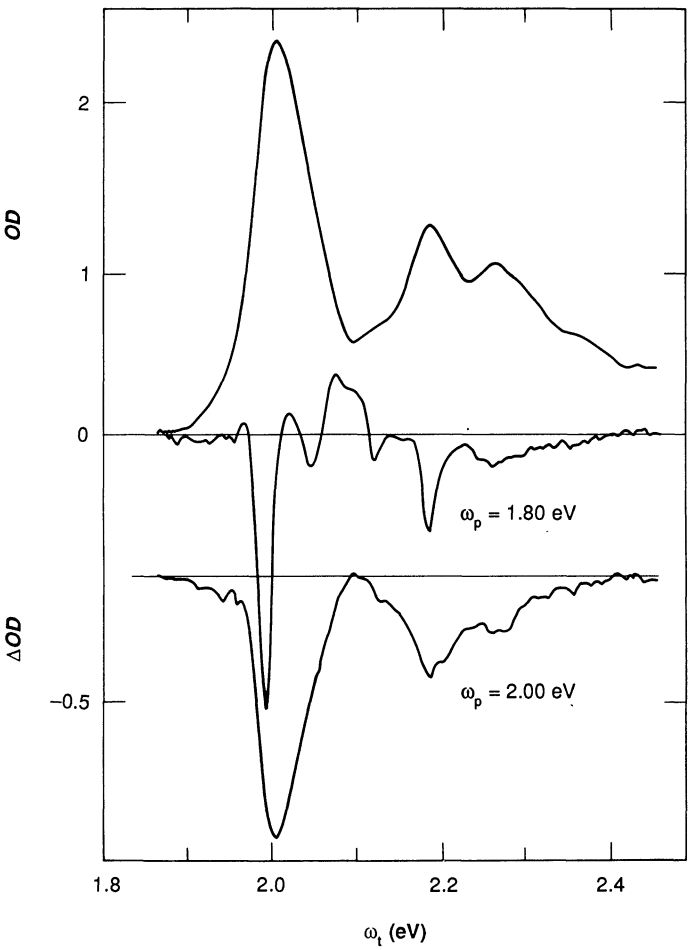

Fig. 4. Optical density of a ~ 200 Å PDA-pTS single crystal film (top). Differential optical density for $\omega_p \sim 1.8$ eV excitation (middle) and resonant $\omega_p \sim 2$ eV excitation (bottom).

coherence is maintained over the entire sample (*21*). However, the actual N dependence of $\chi^{(3)}$, which results from the interplay of large dipole moments, correspondingly large superradiant decay rates ($\sim N$), proper dephasing and laser detuning, is rather complicated. As demonstrated recently for Frenkel excitons, $\chi^{(3)}$ does not show in general a universal enhancement with system size, and under off-resonant conditions it strictly scales like the individual atom result $\sim N$ (*22*). The PSF model in its present form completely ignores superradiant effects, so that $\chi^{(1)}$ and $\chi^{(3)}$ always scale like the concentration of atoms.

Upon comparing Eq. 16 with the two-level system result Eq. 3, we can immediately write down the third-order optical Bloch equations including Coulomb effects (*6*)

$$\frac{\partial}{\partial t}P_k^{(3)}(t) = -i(\epsilon_{ck} - \epsilon_{vk})P_k^{(3)}(t) - 2i|\mu|^2 f_k^{(2)}(t)E(t) + i\sum_{k'} V_{k,k'}P_{k'}^{(3)}(t) - \gamma_2 P_k^{(3)}(t) + \text{exciton-exciton interactions} \quad (21)$$

and

$$\frac{\partial}{\partial t}f_k^{(2)}(t) = i[P_k^{(1)*}(t)\Delta_k^{(1)}(t) - P_k^{(1)}(t)\Delta_k^{(1)*}(t)] - \gamma_1 f_k^{(2)}(t) + \text{exciton-exciton interactions} \quad (22)$$

where

$$|\mu|^2\Delta_k^{(1)}(t) = |\mu|^2 E(t) + \sum_{k'} V_{k,k'}P_{k'}^{(1)}(t) \quad (23)$$

is the self-consistent "local" field to which the system responds. Here, we have separated the two-level system-like anharmonic exciton-photon interaction from the exciton-exciton one, which shall not concern us here. (Since almost no exact results are known, neglect of the latter can usually only be justified empirically.)

Theoretical studies of Eqs. 21 to 23 for 2-D and 3-D systems (including some exciton-exciton interactions) abound in the literature (*6*) and we shall limit ourselves to those aspects pertinent to our experiments. For a single monochromatic pump field $E(t) = E_p\exp(-i\omega_p t)$ and keeping only the lowest exciton term, one finds after some straightforward algebra

$$\chi_p^{(3)}|E_p|^2 = -\chi_p^{(1)}\frac{2\sum_k f_k^{(2)}\phi_x(k)}{\sum_k \phi_x(k)} \quad (24)$$

where

$$f_k^{(2)} = \frac{N|\mu E_p\phi_x(k)\phi_x^*(z=0)|^2}{(E_x-\omega_p)^2+\gamma_2^2}\frac{2\gamma_2}{\gamma_1} \quad (25)$$

is the induced excited state population. Apart from the exciton orbital wave functions, this result is identical to the two-level system result Eq. 11. Introducing the total exciton number $N_x = \sum_k f_k^{(2)}$, Eq. 25 may also be written in the form

$$f_k^{(2)} = N_x|\phi_x(k)|^2 \quad (26)$$

Thus, the third-order susceptibility due to anharmonic exciton-photon interaction is of the simple saturation form

$$\chi_p^{(3)}|E_p|^2 = -\chi_p^{(1)}\frac{N_x}{N_s} \quad (27)$$

where

$$N_s^{-1} = \frac{2\sum_k |\phi_x(k)|^2\phi_x(k)}{\sum_k \phi_x(k)} \quad (28)$$

is the so-called saturation parameter (*6*).

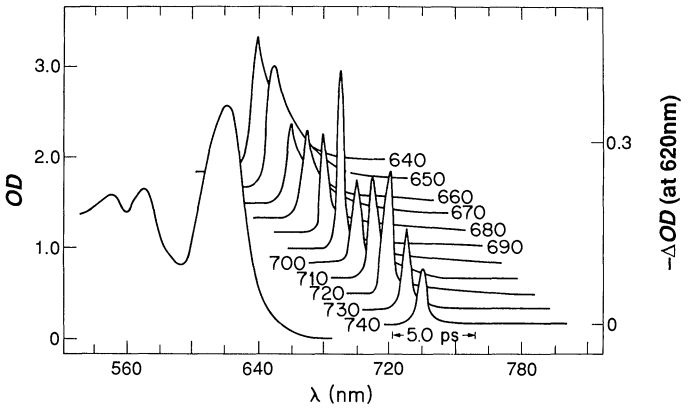

Fig. 5. Optical density (left) and time-resolved differential optical density (right), measured at $\omega_t \sim 2$ eV, for various pump wavelengths. Spectra are displaced, with the temporal peaks positioned above the excitation wavelength at which they were taken.

Equations 24 to 28 have the following intuitive interpretation: in the presence of a finite exciton population N_x, some of the single-particle Bloch states needed to form the exciton state are already occupied, with a probability distribution given by the exciton orbital wave function and number (Eq. 26). Due to the Pauli exclusion principle, this yields then a reduction in exciton oscillator strength (Eq. 24). Put another way, saturation sets in when excitons start to overlap.

The Fourier transform of the exciton wave function Eq. 19 is

$$\phi_x(k) \sim 2\left(\frac{a_x}{Na}\right)^{1/2}\frac{1}{1+k^2a_x^2} \quad (29)$$

which yields $N_s^{-1} \sim (3a_x)/(Na)$. This intuitive result is reduced by a factor of 2, if spin degrees of freedom are included. As in higher dimensions, the saturation density is thus simply the inverse of the exciton volume (*6, 23*).

The data shown in Fig. 4 indicate a uniform exciton bleaching consistent with Eq. 27. Note that under our experimental conditions (ultrashort optical pulses, ultrafast dephasing, and positive time delay), the coherent population modulation term does not contribute, so that Eq. 27 may also be used for the susceptibility experienced by the test beam, provided we substitute the actual exciton number N_x at the delay ~ 0.2 ps (*24*). From the measured fractional change in peak absorption $\Delta OD/OD \sim -N_x/N_s \sim -0.2$, we find a 1-D exciton Bohr radius of $a_x \sim 30$ to 40 Å. This value is consistent with values obtained from time-resolved reflectivity (*23*) and photoacoustic measurements of absorption saturation in Langmuir-Blodgett films of PDA-pTS (*25*). Independent evidence for an exciton Bohr radius of this size comes from a first principles calculation (*26*) and from experiments in which short chain segments of varied length were synthesized (*27*). For chains shorter than about five unit cells (~ 25 Å), a dramatic increase in exciton energy is found, due to quantum confinement. This effect is analogous to the increase in exciton energy which takes place in quantum well structures when the well size becomes comparable to the bulk exciton Bohr radius (*6*).

Since the exciton number N_x varies according to Eqs. 18 and 25 like the linear absorption, that is, like $(Na)/a_x$, the ratio of $\chi_p^{(3)}$ to $\chi_p^{(1)}$ is actually independent of exciton size and close to that of the underlying atomic transition (apart from the different dephasing in a solid). This demonstrates a very fundamental point: for exciton creation, the nonlinear changes per photo-excited e-h pair are essentially independent of material and dimensionality (*6*). This is

also a well-known empirical fact (*12*). The available absolute changes increase (like the linear absorption) as one proceeds say from GaAs to PDA-pTS (by two orders of magnitude), because of the decrease in exciton size. However, the saturation density increases by the same amount, and the two effects exactly cancel.

The above arguments may be extended to nonresonant excitation well below the exciton resonance to describe the nonresonant nonlinear refractive index n_2 and the excitonic ac Stark effect recently observed in pump and probe experiments in GaAs-based systems (*6*) and PDA-pTS (*19*). While the quantitative description of GaAs-based systems may require extensive numerical work (for instance, for large pump detunings virtual e-h pairs do not live long enough to form bound states and sums over all exciton states have to be taken), the situation is much simpler in PDA-pTS. This is because even for large detunings of ~1 eV the lowest exciton state still dominates the physics, due to its large binding energy and oscillator strength.

By noting that below the exciton resonance the proper dephasing diminishes in an exponential fashion (Urbach's rule), we may set $\gamma_1 = 2\gamma_2$ in Eq. 25 to obtain the nonresonant third-order susceptibility at large detuning ($E_x - \omega_p >> \gamma_2$)

$$\chi_p^{(3)}|E_p|^2 = -\frac{N}{V}\frac{|\mu\phi_x(z=0)|^2}{E_x-\omega_p}\frac{N_x}{N_s} \tag{30}$$

where

$$N_x = \frac{N|\mu E_p\phi_x(z=0)|^2}{(E_x-\omega_p)^2} \tag{31}$$

From these expressions, one finds a nonresonant nonlinear refractive index $n_2 \sim 10^{-12}$ cm^2 W^{-1}, in excellent agreement with the reported experimental value (*5, 10*).

The steady-state third-order susceptibility $\chi_t^{(3)}$ experienced by a weak probe beam may be derived in the same fashion as Eq. 12 (*6*). From the population modulation term $[\Delta f_k^{(2)}]$, one obtains an ac Stark shift of the exciton which, not surprisingly, is basically the same as that of the underlying atomic transition (for the same pump detuning).

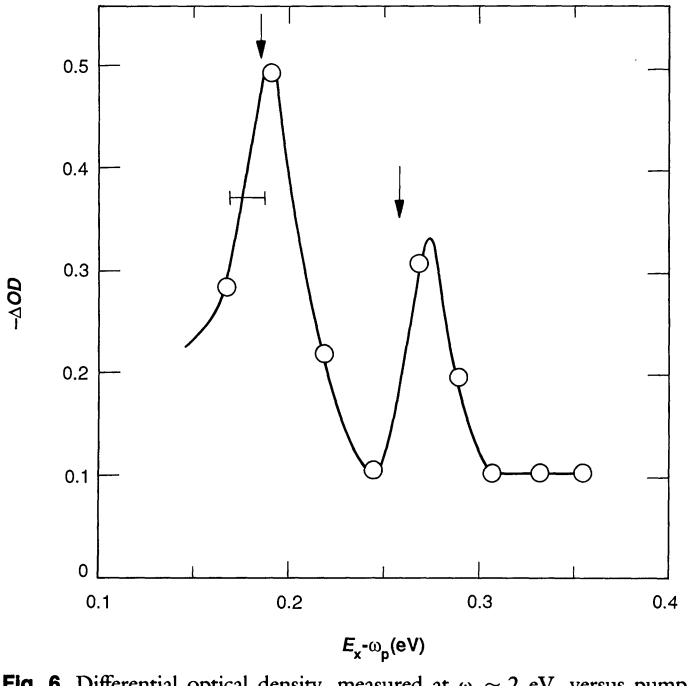

Fig. 6. Differential optical density, measured at $\omega_t \sim 2$ eV, versus pump detuning from the exciton resonance $E_x - \omega_p$. Horizontal bar indicates pump spectral bandwidth. Solid line through data (circles) serves only as a guide to the eye. Arrows indicate optic phonon energies obtained from resonant Raman spectroscopy.

The quantitative success of the simple PSF model in describing resonant and nonresonant experiments without adjustable parameters suggests that it contains the correct physics underlying most of the nonlinear optical response of PDA-pTS. This obviously does not include the off (but near) resonant ($\omega_p \sim 1.8$ eV) data shown in Figs. 4 to 6, which we shall discuss now.

First we note that the differential optical density shown in the center of Fig. 4 differs dramatically from what one might expect for two-level–like systems (Fig. 3b) and what has been observed in analogous experiments on GaAs (*6*). Rather, a narrow hole is "burned" into the exciton line, similar to the "coherent artifact" in Fig. 3a. The magnitude of this hole increases with pump intensity, reaching a fractional change of $\Delta OD/OD \sim -0.2$ at our highest intensity $I_p \sim 3$ GW cm^{-2}. The dependence of the nonlinear optical response on the pump detuning is also remarkable: instead of a monotonic decrease with pump detuning, optic phonon resonances are observed (Figs. 5 and 6).

These experimental findings indicate that the nonlinear optical response near (but below) the exciton resonance in PDA-pTS is dominated by an anharmonic interaction between excitons mediated by optic phonons, that is, stimulated phonon exchange between pump and probe beam by way of intermediate exciton states. This effect, the generation of a nonlinear signal at a test frequency $\omega_t = \omega_p + \omega_o$ (ω_o is the optic phonon frequency), has been first observed in organic molecule solutions and is usually referred to as "inverse (anti-Stokes) Raman scattering" (*28*). In the context of inorganic bulk semiconductors, it was independently discussed by Ivanov and Keldysh who also gave it a different name: formation of "phonoritons," mixed excitations consisting of phonons, excitons, and photons (polaritons) (*29*). We note that experimental evidence of the existence of this effect in semiconductors has been reported for a variety of materials with strong exciton-phonon interaction. Related phenomena have also been observed in Cu_2O and GaAs quantum wells, but with the optic phonons replaced by an intra-excitonic (*30*) or intersubband (*31*) excitation.

In molecular physics, the inverse Raman effect is often explained in terms of a resonant ac Stark effect in a three-level system, consisting of ground zero–phonon (|0>), ground one–phonon (|1>), and excited zero–phonon (|x>) states (Fig. 7) (*32*). The pump, which is resonant with the ground one–phonon to excited zero–phonon transition, induces an ac Stark splitting of the latter, which is probed by the test beam. Thus, in this simple picture, the exciton line splits into two, which qualitatively accounts for the data shown in the center of Fig. 4.

The resonant linear and third-order susceptibilities for the three-level system shown in Fig. 7 are given by (*32*)

$$\chi_t^{(1)} = \frac{|\mu_{0x}|^2}{E_x - \omega_t - i\gamma_2} \tag{32}$$

and

$$\chi_t^{(3)}|E_p|^2 = \chi_t^{(1)}\frac{|\mu_{1x}E_p|^2}{(E_x - \omega_t - i\gamma_2)(\omega_p + \omega_o - \omega_t - i\gamma_o)} \tag{33}$$

where γ_o^{-1} is the phonon lifetime and μ_{0x} (μ_{1x}) the dipole matrix element for the ground zero–phonon (one-phonon) to excited zero–phonon transition. These expressions form the beginning of a geometric series, which may be readily summed to give the nonlinear optical susceptibility experienced by a weak probe beam (*32*)

$$\chi_t = |\mu_{0x}|^2/\left[E_x - \omega_t - i\gamma_2 - \frac{|\mu_{1x}E_p|^2}{\omega_p + \omega_o - \omega_t - i\gamma_o}\right] \tag{34}$$

This result is valid for any strength of the pump field E_p and clearly displays the phonon-mediated ac Stark effect for $\omega_p + \omega_o = E_x$.

We have developed a slightly different microscopic model, the results of which are shown in Fig. 8 for parameters appropriate to PDA-pTS and our experimental conditions (*18*). The full lines give the imaginary part of χ_t and the dashed lines the real part. In Fig. 8, a and b, the pump is exactly one phonon energy below the center of the exciton line, $\omega_p + \omega_o = E_x$. In agreement with experiment, narrow holes appear in $\mathrm{Im}\chi_t$, which increase with pump intensity. When the inverse Raman resonance $\omega_p + \omega_o$ is in the wing of the exciton line (Fig. 8c), the nonlinear feature in $\mathrm{Im}\chi_t$ becomes smaller and acquires a dispersive shape. Finally, for $\omega_p + \omega_o$ below the exciton resonance (Fig. 8d), it changes back to absorptive. These dramatic changes in lineshape already follow from Eq. 33 and have been recently observed in PDA-pTS (*18, 19*). The theoretical spectrum Fig. 8a corresponds to our experimental conditions, Fig. 4 center, and reproduces the general features and magnitude of the observed effect. The remaining discrepancies, such as the width and slight red shift of the hole, are not surprisingly in view of the neglect of dispersion, electronic ac Stark effect, excited one-phonon states, temporal evolution, and spectral width of the pulses.

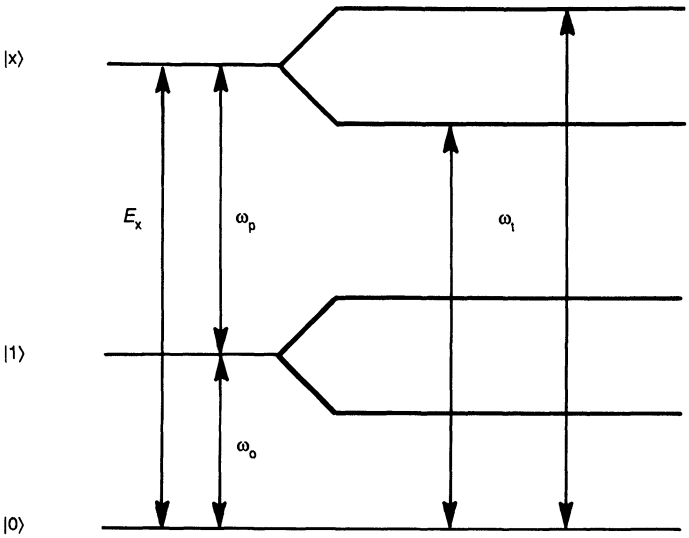

Fig. 7. Three-level configuration for phonon-mediated ac Stark effect.

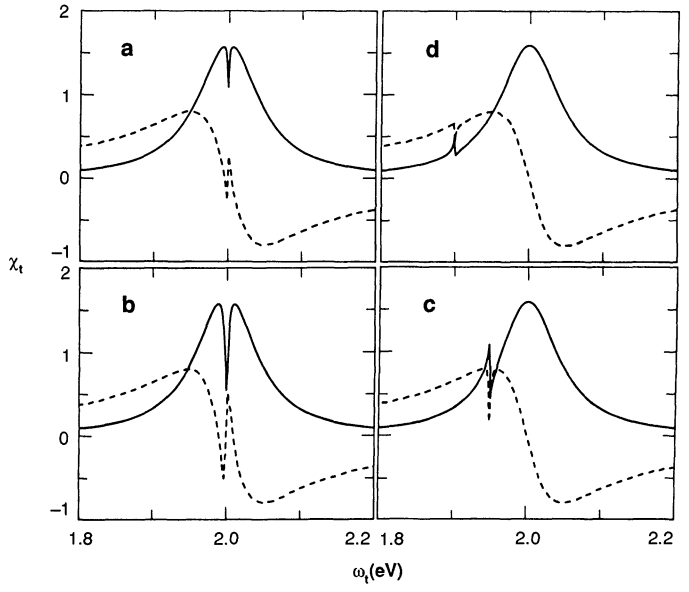

Fig. 8. Real (dashed lines) and imaginary (full lines) parts of the susceptibility χ_t experienced by a monochromatic test beam in the presence of a monochromatic pump beam, for various pump frequencies ω_p and intensities I_p: (**a**) ω_p = 1.8 eV and I_p = 3 GW cm^{-2}, (**b**) ω_p = 1.8 eV and I_p = 6 GW cm^{-2}, (**c**) ω_p = 1.75 eV and I_p = 6 GW cm^{-2}, (**d**) ω_p = 1.7 eV and I_p = 6 GW cm^{-2}.

Conclusions and Future Directions

The simple arguments based on saturation effects presented above provide the framework on which to base expectations for "all-optical" nonlinearities in both organic and inorganic materials. With regard to resonant effects, we have argued that all materials possessing allowed low-lying electronic transitions will exhibit essentially equal magnitude nonlinear optical responses per photoexcited electron-hole pair. This fact is derived from the inverse relationship between the oscillator strength of an elementary electronic excitation and its physical size, together with the absolute limit on oscillator strength per unit volume derived from the atomic origin of matter/f-sum rule.

Practical considerations of photochemical stability, however, strongly disfavor the use of organics for resonant device application. From the collective experience of literally thousands of years of experimentation with dyes and pigments, it is known that even the most photochemically stable molecules fall far short of what would be needed for high bit-rate device application. A sizable change in optical constants requires a significant photoinduced population change. This implies that a large fraction of the molecules in the active region of the device must absorb a photon during every binary operation. At proposed bit rates of 10^9 s^{-1}, assuming a conservative quantum yield for photodegradation of a typical organic chromophore of 10^{-8}, the device would self-destruct in 10^{-1} s (*33*).

Inorganic semiconductors (such as GaAs) are fundamentally different in this regard. While organics typically have electronic states of higher spin multiplicity lying below the first excited electronic singlet state, inorganic semiconductors have no intrinsic electronic states within the energy gap. Triplet states in molecules, generated either photochemically or thermally, are well known to be photochemically reactive. This is not an issue of sample purity. Organics are photochemically unstable by comparison to inorganic semiconductors.

The practical considerations concerning nonresonant device applications are considerably different. Here, the real figure of material merit is n_2/α, reflecting the deleterious effect of residual absorption on device performance. We have shown that the nonresonant nonlinearity can be related to the absorption strength in a low-lying electronic transition by means of the construct of absorption saturation by creation of virtual excitations (*6, 23*). We have also argued that one aspect determining n_2 is bounded by sum rules, namely the total integrated strength of an optical transition cannot become arbitrarily large. The ideal nonresonant nonlinear material is therefore one in which a maximally intense low-lying electronic absorption can be approached to arbitrary degree from below (lower frequency) without significant linear (or higher order) absorption.

An examination of the transparency characteristics of a variety of solids shows, for example, SiO_2 and the alkali halides obtaining values of the absorption coefficient α as low as 10^{-3} to 10^{-6} cm^{-1} in the near- to mid-infrared region of the spectrum (*34*). These absorptions are attributable to phonon overtones. Ultra-transparent materials have their fundamental phonon frequencies at ~500 cm^{-1} and below, which would require extremely high order (low probability) processes to result in absorption at ~10^4 cm^{-1}. By compari-

son, PDA-pTS has phonon frequencies as high as ~2000 cm^{-1}, with discrete overtone absorption features apparent in the near infrared, and a minimum absorptivity in its "transparent" region of roughly ~1 cm^{-1} (*35, 36*). By the criterion of n_2/α, SiO_2 and PDA-pTS are roughly comparable.

As it stands today, there have been no high-speed device demonstrations based on a nonresonant electronic all-optical nonlinear effect in an organic material. Well-established values of n_2 and α would lead one to expect thermal and electronic effects to be of comparable magnitude, depending to some degree on peak light intensities, duty cycle, wavelengths, and thermal parameters of the specific device and active materials (*12, 35–38*).

The allure of nonresonant optical nonlinearities in organics has been the notion that the effects are large, fast, and effectively "free" with respect to energy deposition in the material. Unfortunately, we have learned that while the effects are fast and relatively large when compared to similar effects in other materials, they are accompanied by a significant amount of absorption. We are ultimately left with a borderline situation with respect to practical device application.

It would appear that it is time to reevaluate efforts toward obtaining organic materials suitable for high-speed all-optical device application. Future work must explicitly address the issues of transparency and its ultimate relationship to spectral lineshapes and strengths. Perhaps it is time to renew interest in the much larger but slower speed effects (photorefractive phenomena, for instance) that are perfectly well-suited to exploit the massive parallelism contemplated with all-optical computational architectures (*39*).

REFERENCES AND NOTES

1. N. Bloembergen, *Nonlinear Optics* (Benjamin, New York, 1965).
2. Y. R. Shen, *The Principles of Nonlinear Optics* (Wiley, New York, 1984).
3. D. S. Chemla and J. Zyss, Eds., *Nonlinear Optical Properties of Organic Molecules and Crystals* (Academic Press, Orlando, FL, 1987).
4. Because all materials absorb some light at all frequencies, the separation of nonlinear optical effects into resonant and nonresonant regimes is only meant to categorize the origin of the dominant nonlinearity.
5. C. Sauteret *et al.*, *Phys. Rev. Lett.* **36**, 956 (1976).
6. S. Schmitt-Rink, D. S. Chemla, D. A. B. Miller, *Adv. Phys.* **38**, 89 (1989).
7. A. J. Heeger, S. Kivelson, J. R. Schrieffer, W. P. Su, *Rev. Mod. Phys.* **60**, 781 (1988).
8. D. Bloor and R. R. Chance, Eds., *Polydiacetylenes* (Nijhoff, Dordrecht, 1985).
9. The second-order susceptibility $\chi^{(2)}$ describes a separate class of nonlinear optical effects, such as second-harmonic generation and the electro-optic effect. While outside the subject matter of this article, the manifestation of these phenomena in organics represents an exciting current field of materials research.
10. G. M. Carter *et al.*, in (*3*), vol 2, p. 85.
11. D. N. Batchelder, in (*8*), p. 187.
12. H. M. Gibbs, *Optical Bistability: Controlling Light with Light* (Academic Press, Orlando, FL, 1985).
13. S. Feneuille, *Rep. Prog. Phys.* **40**, 1257 (1977).
14. B. R. Mollow, *Phys. Rev. A* **5**, 2217 (1972).
15. R. W. Boyd and S. Mukamel, *ibid.* **29**, 1973 (1984).
16. B. I. Greene, J. Orenstein, R. R. Millard, L. R. Williams, *Chem. Phys. Lett.* **139**, 381 (1987).
17. G. M. Carter, J. V. Hryniewicz, M. Thakur, Y. J. Chen, S. Meyler, *Appl. Phys. Lett.* **49**, 998 (1986).
18. B. I. Greene *et al.*, *Phys. Rev. Lett.* **61**, 325 (1988).
19. G. J. Blanchard *et al.*, *ibid.* **63**, 887 (1989).
20. R. J. Elliott, *Phys. Rev.* **108**, 1384 (1957).
21. E. Hanamura, *Phys. Rev. B* **37**, 1273 (1988).
22. F. C. Spano and S. Mukamel, *Phys. Rev. A*, in press.
23. B. I. Greene, J. Orenstein, R. R. Millard, L. R. Williams, *Phys. Rev. Lett.* **58**, 2750 (1987).
24. C. H. Brito Cruz, J. P. Gordon, P. C. Becker, R. L. Fork, C. V. Shank, *IEEE J. Quantum Electron* **24**, 261 (1988).
25. F. Kajzar *et al.*, *Opt. Commun.* 66, 55 (1988).
26. S. Suhai, *J. Chem. Phys.* **85**, 611 (1986).
27. F. Wudl and S. P. Bitler, *J. Am. Chem. Soc.* **108**,. 4685 (1986).
28. W. J. Jones and B. P. Stoicheff, *Phys. Rev. Lett.* **13**, 657 (1964).
29. A. L. Ivanov and L. V. Keldysh, *Zh. Eksp. Teor. Fiz.* **84**, 404 (1982) [*Sov. Phys. JETP* **57**, 234 (1983)].
30. D. Froehlich, A. Noethe, K. Reimann, *Phys. Rev. Lett.* **55**, 1335 (1985).
31. D. Froehlich, R. Wille, W. Schlapp, G. Weimann, *ibid.* **59**, 1748 (1987).
32. S. Saikan, N. Hashimoto, T. Kushida, K. Namba, *J. Chem. Phys.* **82**, 5409 (1985).
33. N. S. Allen and J. F. McKellar, *Photochemistry of Dyed and Pigmented Polymers* (Applied Science, London, 1980).
34. S. S. Mitra and B. Bendow, Eds., *Optical Properties of Highly Transparent Solids* (Plenum, New York, 1975).
35. W. Krug, E. Miao, M. Derstine, J. Valera, *J. Opt. Soc. Am. B* 6, 726 (1989).
36. M. Thakur, R. C. Frye, B. I. Greene, in preparation.
37. J. M. Nunzi and D. Grec, *J. Appl. Phys.* 62, 2198 (1987).
38. G. I. Stegeman, R. Zanoni, C. T. Seaton, in *Nonlinear Optical Properties of Polymers*, A. J. Heeger, J. Orenstein, D. R. Ulrich, Eds. (Materials Research Society, Pittsburgh, 1988), p. 53.
39. P. Guenter and J. P. Huignard, Eds., *Photorefractive Materials and Their Applications* (Springer, New York, 1988).

40. The authors gratefully acknowledge the help of M. Thakur, R. R. Millard, L. R. Williams, D. H. Rapkine, and J. F. Mueller, who have contributed to this research effort over the past few years.